RSC Advances

ROYAL SOCIETY OF CHEMISTRY

www.rsc.org/advances

Cite this: DOI: 10.1039/c0xx00000x

www.rsc.org/xxxxxx

ARTICLE TYPE

Graphical abstract

DNA binding, molecular docking and apoptotic inducing activity of nickel(II), copper(II) and zinc(II) complexes of pyridine-based tetrazolo[1,5-*a*]pyrimidine ligands

A. Haleel,[a] P. Arthi,[a] N. Dastagiri Reddy,[b] V. Veena,[c] N. Sakthivel,[c] Y. Arun,[d] P.T. Perumal,[d] A. Kalilur Rahiman[a]*

Graphic

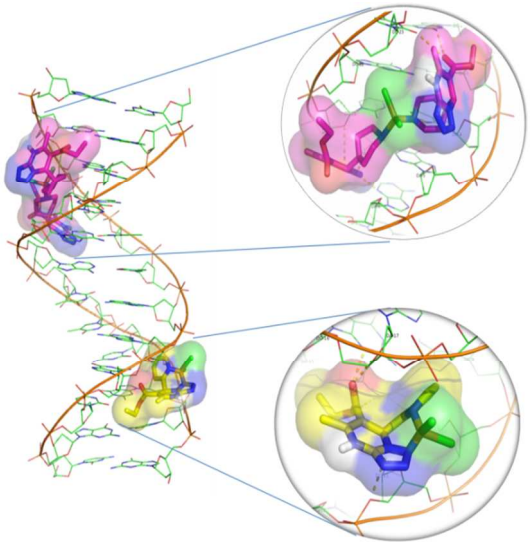

Highlights

The biological activity of metal(II) complexes of tetrazolo[1,5-*a*]pyrimidine ligands show that the copper(II) complexes may act as promising anticancer agents.

Cite this: DOI: 10.1039/c0xx00000x

www.rsc.org/xxxxxx

ARTICLE TYPE

DNA binding, molecular docking and apoptotic inducing activity of nickel(II), copper(II) and zinc(II) complexes of pyridine-based tetrazolo[1,5-*a*]pyrimidine ligands

A. Haleel,[a] P. Arthi,[a] N. Dastagiri Reddy,[b] V. Veena,[c] N. Sakthivel,[c] Y. Arun,[d] P.T. Perumal,[d] A. Kalilur Rahiman[a]*

Received (in XXX, XXX) Xth XXXXXXXXX 20XX, Accepted Xth XXXXXXXXX 20XX
DOI: 10.1039/b000000x

Six mononuclear nickel(II), copper(II) and zinc(II) complexes, $[ML^1Cl_2]$ (**1**–**3**) and $[M(L^2)_2Cl_2]$ (**4**–**6**), of two biologically active tetrazolo[1,5-*a*]pyrimidine core ligands, ethyl 5-methyl-7-pyridine-2-yl-4,7-dihydrotetrazolo[1,5-*a*]pyrimidine-6-carboxylate (L^1) and ethyl 5-methyl-7-pyridine-4-yl-4,7-dihydrotetrazolo[1,5-*a*]pyrimidine-6-carboxylate (L^2), have been synthesized and characterized. The molecular structure of ligands ($L^{1\&2}$) and complex **6** were determined by single crystal X-ray diffraction method. X-ray crystal structure of **6** confirms the distorted tetrahedral structure with ZnN_2Cl_2 coordination environment. All the complexes exhibit an unusual strong luminescence at room temperature. EPR spectra of copper(II) complexes (**2** & **5**) show four lines, characteristic of square planar geometry, with nuclear hyperfine spin 3/2. DNA binding studies of complexes with calf-thymus DNA suggest that complexes **2** and **5** bind in the grooves of DNA. These results were further supported by molecular docking studies. *In vitro* cytotoxic activities of ligands ($L^{1\&2}$) and complexes (**1**–**6**) aganist human cancer cell lines such as lung (A549), cervical (HeLa), colon (HCT-15) and a non-cancer human embryonic kidney (HEK) cell line revealed that the complexes selectively inhibit the growth of cancer cells and inactive against non-cancer cell lines, whereas the ligands were found to be inactive with both cancer and non-cancer cell lines. The IC_{50} values of complexes revealed that the copper(II) complexes (**2** & **5**) exhibit high cytotoxic activity against colon (HCT-15) cells when compared to the standard drug cisplatin. Furthermore, the live cell and fluorescent imaging of cancer cells show that the complexes **2** & **5** induces cell death through apoptosis.

Introduction

A great deal of attention has been devoted towards the synthesis of functional compounds containing polyazole rings, particularly tetrazoles and their derivatives. The synthesis of tetrazoles by traditional cycloaddition reaction needs the usage of expensive and toxic metal-organic azides, suffer from severe water sensitivity, or the use of hydrazoic acid, which is extremely toxic, volatile, explosive and takes long reaction time at 100–125 ºC.[1-3] A safe, convenient, and environmentally friendly synthetic route to synthesize 5-substituted 1*H*-tetrazoles using water as a solvent and zinc salts as catalyst was achieved by Demko and Sharpless.[4] Putting aside the mechanism of [2+3] cycloaddition and *in situ* hydrothermal method, the tetrazole ligand has been shown to be able to participate in at least nine distinct types of coordination modes with metal ions in the construction of metal–organic frame works.[5] Tetrazole with pyridyl functionality group has attracted a growing amount of attention these years in coordination chemistry due to the aromaticity of pyridyl group and excellent coordination ability of the four nitrogen atoms of tetrazole ring, which may act as either a multidentate or a bridging block in supramolecular assemblies.[6, 7]

Nowadays considerable attention has also been diverted towards the synthesis of pyrimidines and related *N*-containing heterocyclic derivatives such as tetrazolopyrimidines. Pyrimidines and fused pyrimidines are the integral part of DNA and RNA and hence play an essential role in several biological and pharmacological activities such as antibiotics, antibacterial, antitumor, cardiovascular etc.[8,9] The formation of tetrazolopyrimidines derived by the condensation of β-diketonoes and β-keto esters with 5-aminotetrazole was first described by Bulow.[10] The tetrazolopyrimidines have been reported to be used in the treatment of obesity, diabetes, atherosclerosis, hypertension, coronary heart disease, hypercholesterolemia, hyperlipidemia, thyroid cancer, hypothyroidism, depression, glaucoma, cardiac arrhythmias and congestive heart failure.[11] In addition to this, the interaction of tetrazolo metal complexes with DNA has been extensively studied due to the site specific binding properties and many fold applications in cancer therapy, these coordination compounds were suitable for DNA secondary structure probes, photoclevers and antitumor drugs.[12] Other than the medicinal application, tetrazolate-based complexes

Cite this: DOI: 10.1039/c0xx00000x

www.rsc.org/xxxxxx

ARTICLE TYPE

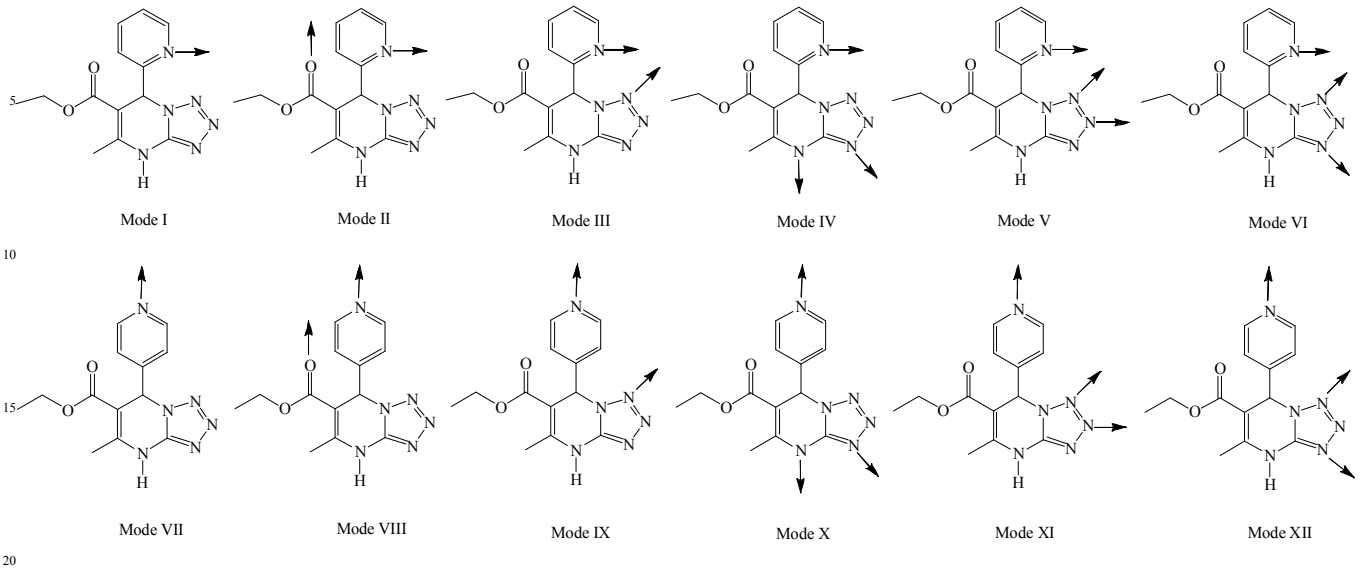

Scheme 1 Possible coordination modes of tetrazolo[1,5-*a*]pyrimidines with metal ions

(5-R-tetrazoles, R = alkyl, pyridyl, phenyl) with transition metals (i.e. Zn, Cd and Cu) were also play an important role in various applications like metal organic coordination polymers (MOCPs), electroluminescence materials (LEDs) and in nonlinear optics.[13-15] Although many investigators are interested in the synthesis of new tetrazolopyrimidine derivatives, there are scarce publications concerning the anti-tumor effects of complexes of tetrazolopyrimidines.

In this context, the coordination of metal ions with tetrazolopyrimidines may be expected to take place in various common coordination modes as shown in **Scheme 1.**[16] To expand this area, we are interested in investigating the use of new tetrazolopyrimidine complexes as potential therapeutic agents, especially as anticancer agents. In this paper, we describe the synthesis, structural characterization, DNA-binding, molecular docking, cytotoxic and apoptotic activities of a new class of mononuclear nickel(II), copper(II) and zinc(II) complexes of two different tetrazolo[1,5-*a*] pyrimidine core ligands, ethyl 5-methyl-7-pyridine-2-yl-4,7-dihydrotetrazolo[1,5-*a*]pyrimidine-6-carboxylate (L^1) and ethyl 5-methyl-7-pyridine-4-yl-4,7-dihydrotetrazolo[1,5-*a*] pyrimidine-6-carboxylate (L^2).

Results and discussion

Synthesis of ligands and complexes

The target ligands $L^{1\&2}$ were synthesized by following the procedure described in the literature.[17] All the complexes (**1-6**) were obtained by the metallation of ligands $L^{1\&2}$ with $NiCl_2$ or $CuCl_2$ or $ZnCl_2$ in methanol. The proposed structure of complexes as shown in **Scheme 2**, was based on spectroscopic investigation as well as elemental analysis and magnetic susceptibility determination.

Description of the crystal structures

The structure of the ligands $L^{1\&2}$ and complex **6** was determined by X-ray analysis and the ORTEP diagrams are given in **Fig. 1-3**. The crystal refinement detail is listed in **Table S1**. Single crystals of $L^{1\&2}$ were obtained by slow crystallization from ethanol. The ligand L^1 crystallized in triclinic space group *P-1* and L^2 crystallized in the orthorhomibic space group *pbca* with inversion centers exhibit planar structure, and the similar arrangement of ligand have been reported in literature.[18] Selected bond length and bond angles are given in **Table S2 & S4**. The NH proton in the pyrimidine ring is involved in intermolecular hydrogen bonding with the nitrogen atom of tetrazole ring of neighboring molecule for the ligand L^1 and with the nitrogen atom of neighboring pyridine ring for the ligand L^2 (**Table S3 & S5**). For the ligand L^1, pyrimidine ring adopts a flattened-boat conformation, with atoms N5 and C2 deviating from the N1/C1/C3/C4 plane by −0.0899 (16) Å and −0.1472 (17) Å, respectively. The N1—N4/C1 and C6—C10/N6 planes form dihedral angles of 5.93 (0.06)° and 86.01 (0.06)°, respectively, with the N1/C1/C3/C4 plane. For the ligand L^2 also the pyrimidine ring adopt flattened-boat conformation, with atoms N5 and C7 deviating from the N5/C6/C4/C5 plane by −0.029 (2) Å and −0.049 (2) Å, respectively. The N2—N5/C6 and C8—C12/N6 planes form dihedral angles of 1.45 (0.08)° and 80.97 (0.08)°, respectively, with the N5/C6/C4/C5 plane (**Fig. S1-S4**).

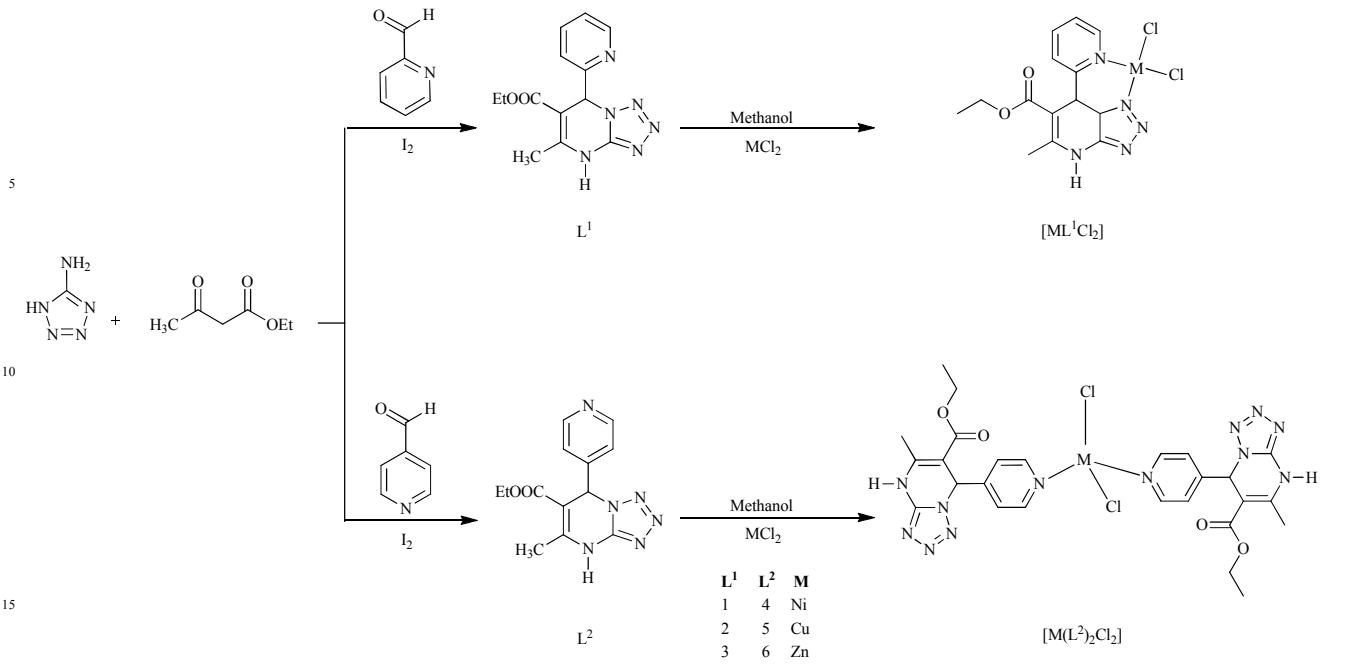

Scheme 2 Schematic route for synthesis of ligands and metal(II) complexes

Small colourless rectangular crystals of complex **6** have been obtained by slow evaporation of a methanolic solution of complex. Selected bond angles and bond length are given in **Table 1**. The crystal system of complex **6** belongs to the monoclinic space group *C2/c* with inversion centre and Zn(II) atoms exhibit a distorted tetrahedral (ZnN_2Cl_2) coordination environment, which is formed by the coordination of two Cl atoms, with a Cl─Zn─Cl bond angle of 118.74(18)°, and more interestingly the zinc atom coordinate to one nitrogen N_1 atom of both the pyridine rings of pyridyl tetrazole which act as a monodentate ligand with a bond angle N(1)─Zn─Cl(1)$^{\#}$ 109.45(19)° and N(1)$^{\#}$─Zn─Cl(1) 109.45(19)°.

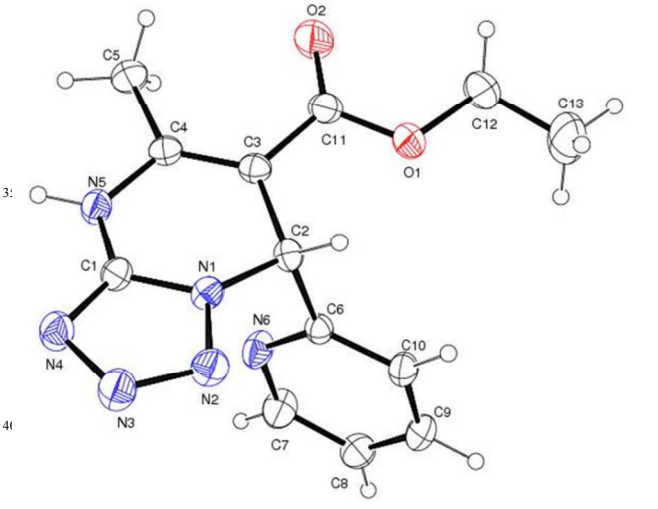

Fig. 1 Single crystal X-ray structure of ligand L^1

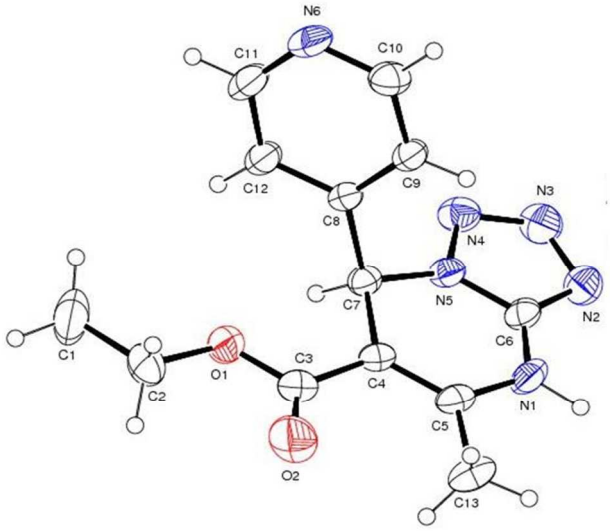

Fig. 2 Single crystal X-ray structure of ligand L^2

The donor *N*-atom forms strong bonds with the zinc atom: the Zn─N(1) bond length is 2.026(6) Å whereas the Zn─Cl(1) bond length is 2.196(3) Å and the C─C, N─N bond distances are comparable to those in analogous systems reported in the literature.[19,20] However, there is a significant twist in the ligand so that the plane of the tetrazole and pyridine rings form dihedral angle of 88.13(2)° with the two independent ligands with respect to zinc metal. The complex forms intermolecular hydrogen bond involving the oxygen atom of carboxylate group O1 of one layer and hydrogen atom of C1 of pyridine group of neighboring layer (**Fig. 4** & **5**) with C(1)─H(1)…O(1)$^{\#}$ distance of 2.66 Å and the nitrogen atom of tetrazole ring N(5)$^{\#}$ will connected by hydrogen bond with the hydrogen atom of N6 of pyridine ring of a neighboring ligand N(6)─H(6)…N(5)$^{\#}$ with distance of 2.05 Å (**Table 2**).

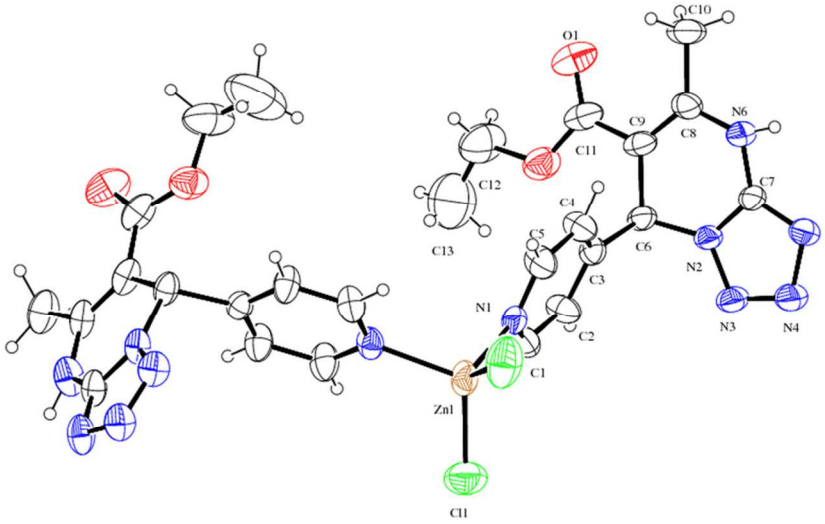

Fig 3 Single crystal X-ray structure of complex **6.**

Table 1 Selected bond lengths (Å) and bond angles (º) for complex **6**.

Bond lengths (Å)			
Cl(1)-Zn(1)	2.195(2)	C(4)-C(5)	1.395(9)
Zn(1)-N(1)$^{\#}$	2.030(5)	C(5)-N(1)	1.335(7)
Zn(1)-Cl(1)$^{\#}$	2.195(2)	C(6)-N(2)	1.460(7)
N(1)-Zn(1)	2.030(5)	C(7)-N(5)	1.309(8)
C(1)-N(1)	1.326(8)	C(8)-N(6)	1.358(8)
C(1)-C(2)	1.363(9)	C(11)-O(1)	1.206(8)
C(2)-C(3)	1.367(7)	C(11)-O(2)	1.320(8)
C(3)-C(4)	1.329(8)	C(12)-C(13)	1.526(19)
C(3)-C(6)	1.538(8)	C(12)-O(2)	1.427(12)
Bond angles (º)			
C(1)-N(1)-Zn(1)	119.4(4)	N(1)-Zn(1)-Cl(1)$^{\#}$	109.41(17)
C(5)-N(1)-Zn(1)	122.7(5)	N(1)$^{\#}$-Zn(1)-Cl(1)	109.40(17)
N(1) -Zn(1)-N(1)$^{\#}$	106.0(3)	N(1)-Zn(1)-Cl(1)	106.18(18)
N(1)$^{\#}$-Zn(1)-Cl(1)$^{\#}$	106.18(18)	Cl(1) -Zn(1) Cl(1)$^{\#}$	119.03(15)

Symmetry transformations used to generate equivalent atoms: #1 —x+2,y,—z+1/2

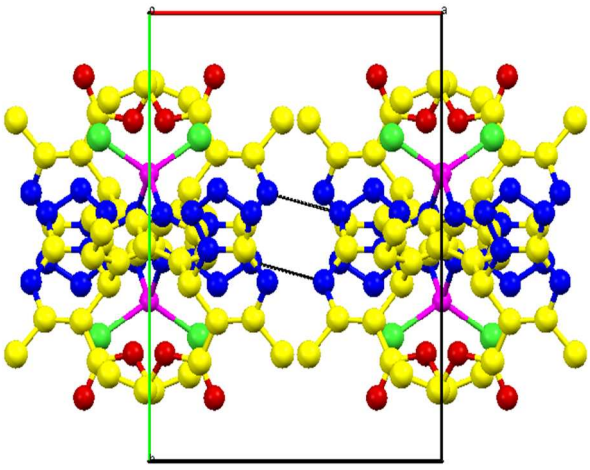

Fig. 4 View of crystal lattice packing showing the internuclear hydrogen bonding of complex **6**.

Table 2 Selected interatomic distance (Å) and angles (º) for complex **6**.

D-H...A	d(D-H) (Å)	d(H...A) (Å)	d(D...A) (Å)	<(DHA) (^{0})
N(6) H(6)...N(5)$^{\#}$	0.82	2.10	2.884(9)	156.2
C(1) H(1)...O(1)$^{\#}$	0.93	2.65	3.310(10)	128.2

Symmetry transformations used to generate equivalent atoms:

#1 —x+2,y,—z+1/2 #2 —x+3,—y+1, —z #3 x—1/2,y—1/2,z

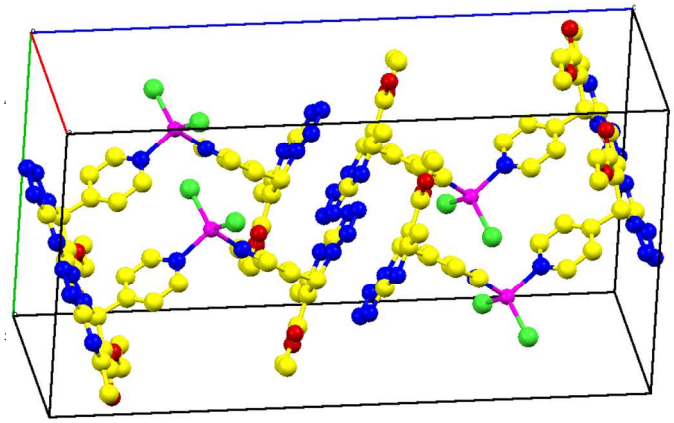

Fig. 5 Crystal packing diagram of complex **6** projecting along the crystallographic *b*-axis.

FT IR spectra

The FT IR spectra of ligands L$^{1\&2}$ show the prominent bands for ν(C=N) of pyrimidine ring and ν(N=N) of tetrazole ring at 1580 and 1553 cm^{-1}, 1447 and 1433 cm^{-1}, respectively. The ligands also show band at 3246 and 3217 cm^{-1}, 1701 and 1721 cm^{-1} assigned for amino and *ν*(C=O) of acetyloxy groups, respectively.[21,22] The complexation was found to result in significant changes in the absorption bands of both ν(C=N) of pyridine and ν(N=N) of tetrazole ring. In the spectra of complexes **1**–**3**, the observed stretching frequency *ν*(C=N) 1559–

1560 cm^{-1} of pyridine ring and ν(N=N) 1420–1429 cm^{-1} of tetrazole ring are lower than that of ligands indicating the coordination of metal ions through nitrogen of pyridyl and N=N of tetrazole rings. For complexes **4–6**, the observed stretching frequency of pyridine ν(C=N) 1502–1530 cm^{-1} are lower than that of ligands, whereas ν(N=N) stretching frequency of tetrazole ring remain unchanged. This may be due to the coordination of metal ions with the nitrogen of pyridyl-substituent and not with the N=N of tetrazole ring (**Fig. S5-S8**). Moreover, significant changes are obvious in the region of stretching and stretching-deformation vibration of the tetrazole ring (1100-900 cm^{-1}). The assignment of bands in the region 420–490 cm^{-1} can be attributed to the coordination of N atoms of both tetrazole and pyrimidine ring ν(M–N). No significant changes in the stretching frequency of ν(C=O) is observed for ligands and complexes, indicating that the carbonyl of acetyloxy group is not bound to metal ion.

NMR spectra

The newly synthesized ligands $L^{1\&2}$ and their zinc(II) complexes (**3** & **6**) were characterized by NMR spectroscopy (**Fig. S9-S16**). The ^{1}H NMR spectrum of complex **6** shows considerable changes in the chemical shifts of the signals of the protons when compared to that of free ligand L^2, whereas complex **3** shows no change in the proton signals with respect to their free ligand L^1. This observation also supports the coordination mode of the ligand L^1 through the *N*-atom of tetrazole ring and the *N*-atom of pyridine ring to the zinc(II) metal center for complex **3** and the ligand L^2 through the *N*-atom of pyridine ring and not with the *N*-atom of tetrazole ring for complex **3**.[23,24] Thus, ^{1}H NMR spectra supports the proposed coordination mode of the ligands with the zinc(II) metal center. The ^{13}C NMR of the compounds confirmed the presence of tetrazole ring with the signal in the region 150.1-148.8 ppm.

UV-Vis spectra

The electronic absorption studies allowed us to gain insight into the possible stereochemistry of these complexes. Electronic spectra of complexes (**1-6**) were obtained in CH_3CN solution (**Fig. S17**). The electronic spectra of nickel(II) complexes (**1** and **4**) display a band around 249 and 274 nm due to intraligand transition (π-π*) or ligand-metal charge transfer transition (n-π*). The bands observed at 462 and 470 nm are attributable to and d-d transition, respectively. This confirms the distorted tetrahedral geometry of nickel(II) complexes.[25,26] The copper(II) complexes (**2** and **5**) also exhibit bands at 259 and 260, 307 and 310 assigned to intraligand (π-π*) and ligand-metal charge transfer transitions (n-π*), respectively. The absorption bands at 464 and 472 nm are due to d-d transitions for complexes **2** and **5**, respectively. These assignments suggest the square planar geometry for Cu(II) complexes under investigation.[27] The zinc(II) complexes (**3** and **6**) exhibit only a high intensity band due to strong charge transfer transition at 275 and 290 nm, respectively, assigned as ligand–metal transition, which indicate the tetrahedral geometry around Zn(II) ions.[28] The absence of band above 400 nm may be due to the lack of metal–ligand charge transfer transition, because of d^{10} electronic configuration of zinc(II) ion. On the basis of IR, NMR, electronic spectral data and X-ray studies, distorted tetrahedral geometry is proposed for nickel(II) and zinc(II) complexes, whereas square planar geometry is proposed for copper(II) complexes.

Luminescence properties

In general, the combination of tetrazole core ligands and transition-metal centers in the coordination frame work can be viewed as an efficient method for obtaining new type of luminescent materials.[29] Herein, the luminescence property of complexes (**1-6**) were carried out in liquid state at room temperature by using CH_3CN (**Fig. 6**). Complexes **1** & **2** exhibit a peak at 409 (3.03 eV) and 400 nm (3.10 eV), respectively. The emission is neither metal-to-ligand transfer (MLCT) nor ligand-to-metal transfer (LMCT) in nature and can be assigned to intraligand fluorescent emission, since a similar emission (λ_{max} = 380-400 nm) is also observed for free ligand L^1.

Instead, complexes **4** and **5** display a strong emission peak at 334 (3.71 eV) and 385 nm (3.22 eV), respectively, and may be assigned to intraligand fluorescent emission with an enhanced fluorescent intensity, which is almost twice that of free ligand L^2 (λ_{max} = 380 nm). The origin of the emissive behavior of these complexes are likely to be due to (π-π*) and (n-π*) transition of pyridyl ring of ligands and suggest direct bonding of metal with C=N of pyridyl ring, and hence less rigid structure but in the case of complexes of L^1, the metal bind with both C=N of pyridine ring and N=N of tetrazole ring, hence comparatively more rigid structure may be assigned. This can be explained by conformational rigidity, thereby reducing the non-radiative decay of intraligand (π-π*) excited state of nickel(II) and copper(II) complexes (**4** and **5**) of L^2.[30, 31]

It is universally acknowledged that metal coordination frameworks with a d^{10} configuration possess excellent luminescence property. The emission spectra of zinc(II) complexes (**3** & **6**) have their emission peaks centered at 342 (3.62eV) and 381 nm (3.25eV), respectively. As we know, it is usually believed that the energy transition of d^{10} complexes is tentatively attributed to the ligation of the ligand to metal center and not metal to ligand transfer.[32]

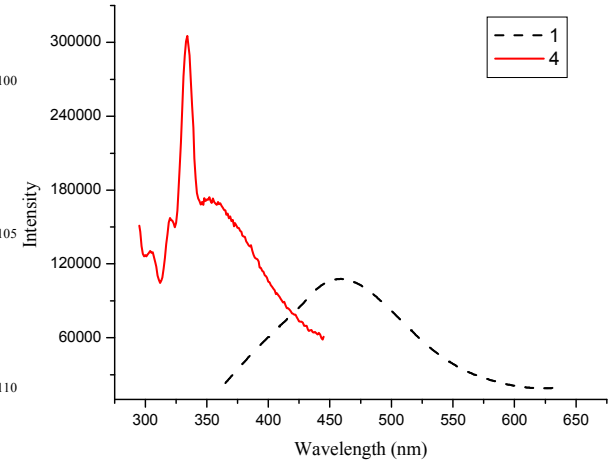

Fig. 6 Emission spectra of complexes **1** and **4** at room temperature.

EPR spectral data

The solid state EPR spectra of copper(II) complexes (**2** & **5**) were recorded in the X-band region at room temperature (25 ºC). **Fig. S18** shows the EPR spectrum of complex **2** and the data are summarized in **Table 3**. Complexes **2** and **5**, exhibit the $g_{\|}$ value of 2.20 & 2.16 and $g_{\perp}$ value of 2.09 & 2.05, respectively. These values indicate that the ground state of Cu(II) is predominantly dx^2-y^2.

The geometric parameter G, which is a measure of the exchange interaction between the copper centers in the polycrystalline compound, is calculated using the equation:

$$G = (g_{\|} - 2.0023)/(g_{\perp} - 2.0023)$$

According to Hathaway and Tomlinson,[33] if G > 4.0 considerable exchange interaction is negligible because the local tetragonal axes are aligned parallel or slightly misaligned. If G < 4.0, exchange is considerable and the local tetragonal axes are misaligned. The observed G values of complexes **2** and **5** (2.25 and 3.30, respectively) suggest that there is no exchange interaction in copper(II) complexes. The covalency parameter α^2 is calculated using the following equation:[34,35]

$$\alpha^2 = (A_{\|}/0.036) + (g_{\|} - 2.0023) + 3/7(g_{\perp} - 2.0023) + 0.04$$

If the value of $\alpha^2 = 0.5$, it indicates complete covalent bonding, while the value of $\alpha^2 = 1.0$ suggests complete ionic bonding. The observed value of α^2 (0.725 and 0.785) of complexes is less than unity, which indicate that complexes have covalent character in the ligand environment.

The two parameters $g_{\|}$ and $A_{\|}$ are to some extent correlated by empirical factor $f = g_{\|}/A_{\|}$.[36,37] Within the related series of compounds, increasing covalency of the metal-ligand bonds leads to decrease in $g_{\|}$ and increase in $A_{\|}$. As the covalency increases, the energies of the excited states rise, so that the orbital contribution to $g_{\|}$ becomes less effective, the $g_{\|}$ becomes closer to the free-electron value. The effect of covalency on the $A_{\|}$ values is impossible to predict, since there are so many factors involved, but theoretical values also suggest that there is a considerable dependence on $A_{\|}$ and $g_{\|}$. The best discrimination is obtained from the parallel values, since this shows the widest variation.[38] All square planar compounds fall in the region shown in **Fig. 7**, with the complexes of softer ligands lying towards the upper part of the band. Distortion towards tetrahedral geometry gives parameters which lie below this band. The ratio $g_{\|}/A_{\|}$ suggests that the Cu(II) complexes lying towards the upper part of the band, suggesting square planar geometry.

Table 3 EPR spectral assignments for complexes **2** and **5** at room temperature

Complexes	$g_{\|}$	$g_{\perp}$	g_{av}	$A_{\|}$ X 10^{-4} (cm^{-1})	F (cm)	α^2	G
2	2.20	2.09	2.12	184.33	119	0.785	2.25
5	2.16	2.05	2.08	183.02	118	0.725	3.30

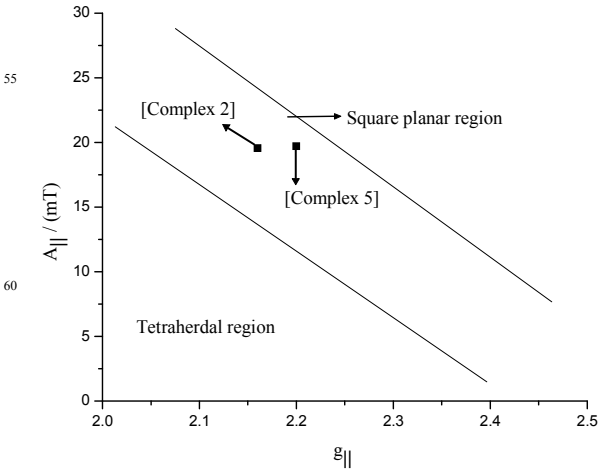

Fig. 7 Correlation between $g_{\|}$ and $A_{\|}$ for complexes **2** and **5**.

Magnetic susceptibility data

The measurement of molar magnetic susceptibility (χ_M) allows us to determine the number of unpaired electrons associated with the transition metal in the compound and useful in understanding the compound's bonding, its magnetic and spectral characteristics. The effective magnetic moment of complexes **2** and **5** are 1.88 and 1.93 BM, respectively, slightly higher than the spin only values (1.73 μ_{eff}) expected for a d^9 system with one unpaired electron.[39] The magnetic moment of Ni(II) complexes **1** and **4** are 3.3 and 3.5 BM. respectively, indicate paramagnetic nature due to tetrahedral geometry around the metal ion.[40] The Zn(II) complexes (**3** and **6**) under study were found to be diamagnetic in nature due to d^{10} system, as expected.

Interaction with calf thymus DNA

Absorption spectral studies

Electronic absorption spectroscopy is widely employed to determine the DNA binding affinity of metal complexes. The absorption spectra of the Cu(II) complexes (**2** and **5**) in the absence and presence of DNA is shown in **Fig. 8.** The absorption bands were affected with increasing concentrations of DNA. A strong hyperchromism along with minor blue shift indicating strong interaction of complexes with CT–DNA mainly through groove binding.[41] DNA possess several hydrogen bonding sites which are accessible both in the major and minor grooves.[42] It is well known that the interactions of chemical species with the minor groove of DNA differ from those occurring in the major groove, both in terms of electrostatic potential and steric effects, because of the narrow shape of the former. For the minor groove the backbone of DNA are closer together with 8.2 Å depth, on the other hand the major groove have the backbones far apart with 11.6 Å width and 8.5 Å depth and offers easy access to bulky molecule.[43,44] Hence, it is easier for certain metal complexes to interact with the bases on the major groove side because the backbone is not in the way. In this context complex **2** may interact to DNA in minor groove due to its little steric interference, compared to complex **5** which may bind to DNA in major groove fashion.[45] In order to compare the DNA-binding

affinities of these complexes quantitatively, their intrinsic binding constants were obtained by monitoring the changes in absorption at intraligand bands (π-π^*) with increasing the concentration of DNA. When the concentration of CT–DNA was increased, a strong hyperchromic effect was observed for complexes **2** and **5**, although no appreciable change in the position of intraligand band was observed. The binding constant (K_b) values are found to be 1.91 X 10^5 M^{-1} and 2.8 X 10^5 $M^{-1}$for complexes **2** and **5**, respectively. The higher hyperchromism and (K_b) value obtained for complex **5** suggest its higher binding affinity to DNA than that for complex **2**. DNA binding studies reveal that both the complexes prefer groove binding; complex **2** binds to CT–DNA through minor groove and complex **5** through major grooves of CT–DNA.

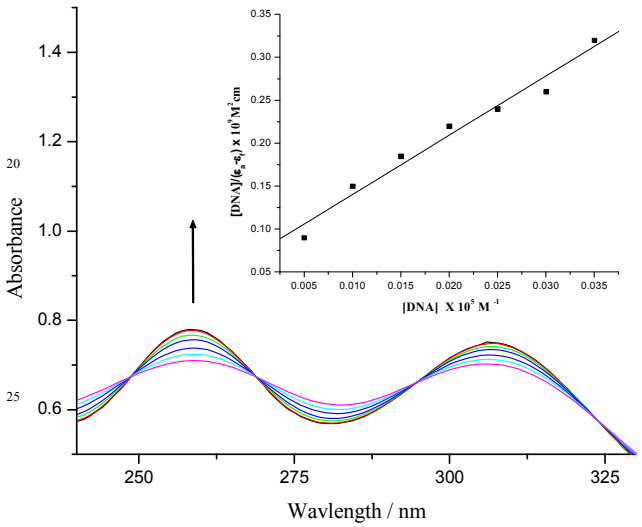

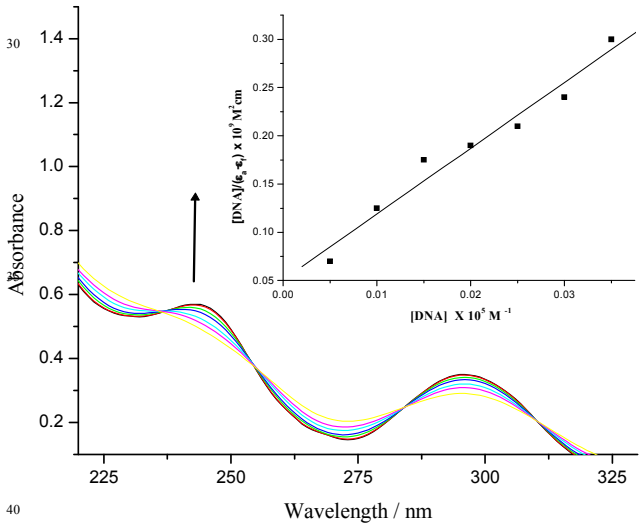

Fig. 8 Absorption spectra of complexes **2** & **5** (10 µM) in Tris-HCl buffer upon addition of CT–DNA (0–100 µM). Arrows indicate the changes in absorbance upon increasing DNA concentration. Inset: plots of [DNA]/(ε_a–ε_f) *versus* [DNA] for absorption titration of CT–DNA with complexes.

Fluorescence quenching studies

To further understand the mode of interaction between the copper(II) complexes (**2** and **5**) with CT–DNA, ethidium bromide (EB) fluorescence displacement experiments were carried out, by monitoring the changes in emission intensity of EB bound to DNA as a function of added complex concentration.[46] The emission spectra of EB bound to DNA in the absence and presence of complexes **2** and **5** are shown in **Fig. 9**. Upon addition of the complexes to DNA pretreated with EB, an appreciable reduction in the DNA-induced emission intensity of EB is caused, indicating the binding of complexes with DNA at the sites occupied by EB. The data were analyzed by using the Stern–Volmer equation. The quenching plots (inset of the respective figures) illustrate that the fluorescence quenching of EB bound to DNA by **2** and **5** is in linear agreement with Stern-Volmer equation, which confirms the interaction of complexes with DNA.

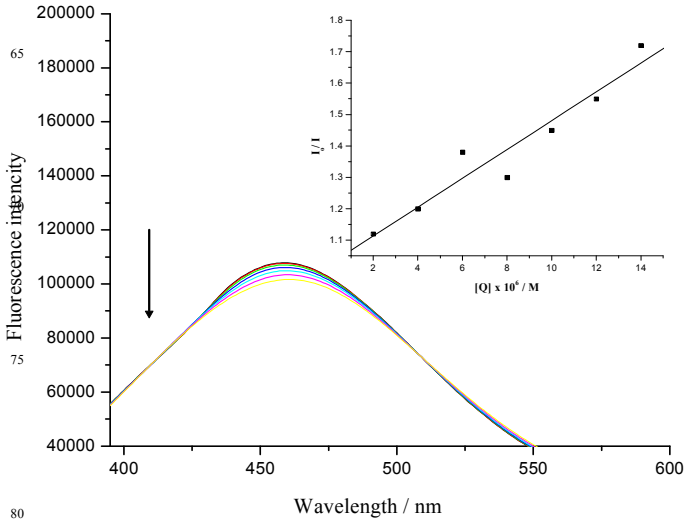

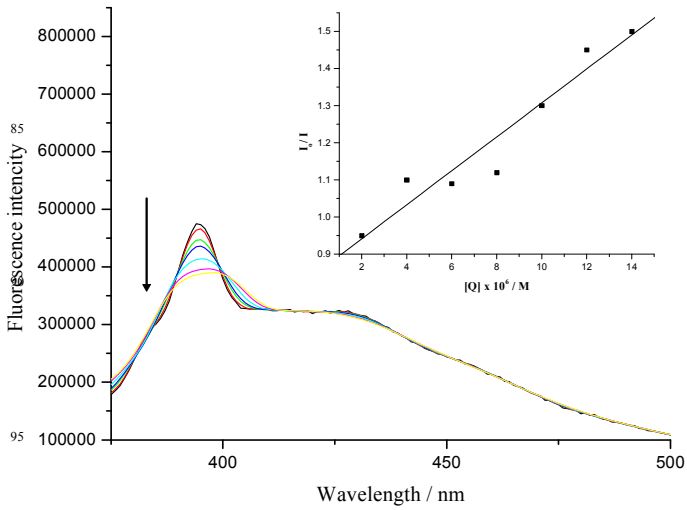

Fig. 9 Fluorescence spectra of complexes **2** & **5** in the absence and presence of increasing amount of complex at 37 ºC: [Complex] = (0-20 µM), [DNA]/[EB] = 10 µM after excitation at λ_{exc} 459 & 393 nm. Inset: plots of I_0/I *versus* [Q] × 10^4/M for the titration of complex with [DNA]/[EB].

The K_{sv} values for **2** and **5** are 0.52 and 1.92, respectively. These values prove the partial replacement of EB bound to DNA by the two complexes which results in decrease in fluorescence intensity. The intrinsic binding parameters clearly show that complexes **2** and **5** strongly interact with CT–DNA. A large increase in emission intensity suggests stronger binding propensity to CT–DNA.

Viscosity measurements

To further clarify the interaction mode of the complexes with DNA, the viscosity measurements were carried out. In classical intercalation, the DNA helix lengthens as the base pairs are separated to accommodate the binding ligand leading to increase in DNA viscosity.[47] In contrast, a partial and/or non-classical intercalation of ligand would bend (or kink) the DNA helix, reducing its effective length and thereby its viscosity, while ligands that binds exclusively in the DNA grooves (e.g., netropsin, distamycin), under the same conditions, typically cause less pronounced changes (positive or negative) or no changes in the DNA viscosity.[48] The plots of relative viscosity $(\eta/\eta_0)^{1/3}$ *versus* binding ratio [Complex]/DNA] is shown in **Fig. 10**.

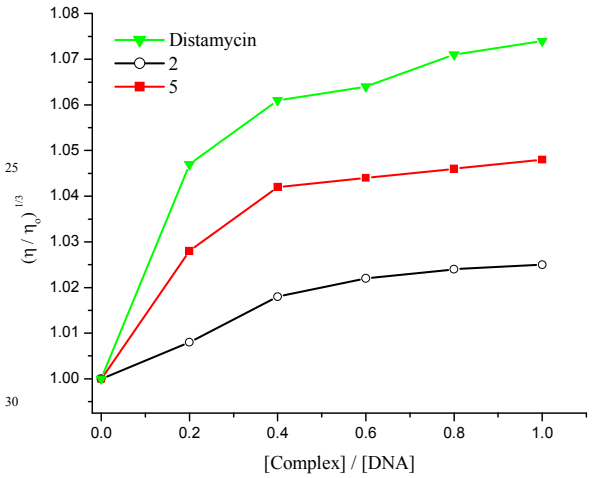

Fig. 10 Effect of the increase in amounts of distamycin (▼), complexes **2**(○) and **5**(■) on the relative viscosity of CT–DNA at 28.0 ± 0.5 ºC

Distamycin, a well known classical groove binder, gave change in DNA viscosity upon complexation. Interstingly, **5** confers an enhancement in DNA viscosity higher than **2**; the hydrophobic interaction of the ligand of the bulkier complex with the DNA major groove, followed by aggregation of the free complex in solution with the DNA-bound complex through the overlap of ligands, lead to untwisting of the DNA helix at the binding sites and hence increase in overall DNA counter length.[49,50] But for **2,** moderate change in viscosity is observed, which is expected to bind with DNA minor grooves. The binding ability of complexes to increase the viscosity of DNA varies in the order **distamycin** > **5** > **2**, which parallels the hyperchromism and DNA binding affinities. The results of this study clearly show that complexes **2** and **5** preferentially bound to DNA through minor and major grooves, respectively. Thus, the viscosity measurements are consistent with the results of the spectral experiments. Therefore, we speculate the groove modes of binding for the two complexes.

Molecular docking of the complexes with DNA.

The molecular docking of the complexes (**2** and **5**) with the self-complementary DNA duplex of sequence dodecamer d(CGCGAATTCGCG)$_2$ demonstrates that the complexes are stabilized by additional electrostatic and hydrogen bonding interaction with the DNA (**Fig. 11**). The Docked conformation of complexes **2** and **5** was analysed in terms of energy, hydrogen bonding, and hydrophobic interaction between complexes with DNA. Detailed analyses of the complex-DNA interactions were carried out, and final coordinates of the complexes and receptor were saved. For display of the receptor with the complex binding site, PyMol software was used. From the docking scores, the free energy of binding (FEB) of the compounds was calculated (**Table 4).** The complexes adopt a characteristic shape and are flexible enough to adopt a conformation which is complementary to the minor and major groove. Molecular docking results of DNA shows that complexes **2** and **5** are bind efficiently with the DNA receptor and exhibits free energy of binding values –8.48 and –9.77 Kcal/mol, respectively. The more negative relative binding energy indicated that complex **5** strongly binds to the DNA than **2**. Because right handed DNA being complimentary to the complex **5** which exhibit strong interaction *via* hydrogen bonding molecular symmetry.[51] The best possible conformation of the mononuclear copper(II) complexes **2** and **5** is through the interaction of tetrazole, pyridine and acetyloxy group of ligand to DNA through minor and major groove, which is due to stabilization by hydrogen bonding. Furthermore, in complex **5**, tetrazole nitrogens interact with DA-6, DC-21 and DT-21 residues, pyridine nitrogen interact with DG-4 residue and carbonyl oxygens of ester substitution interact with DG-2 and DC-23 residues of DNA and in complex **2**, tetrazole nitrogen interact with DC-11 residue, carbonyl oxygens of ester substitution interact with DA-16 and DA-17 residues and oxygen of ester substitution interact with DG-10 residue of DNA. Thus, we can conclude that molecular docking studies provide additional evidence for the preferred minor and major groove modes of binding with the copper(II) complexes.

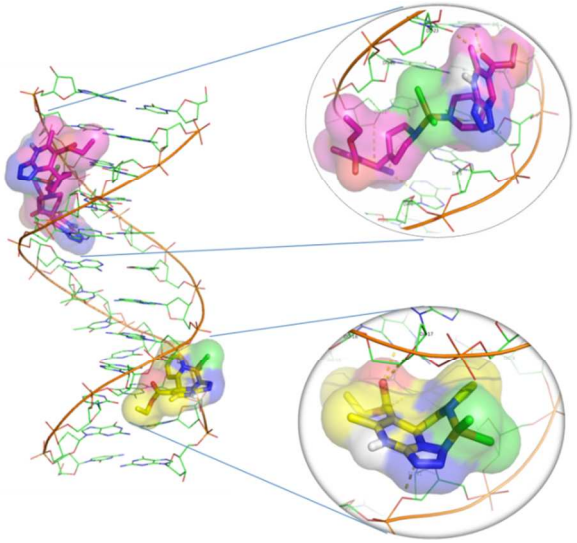

Fig. 11 Molecular docked model of complexes **2** and **5** with DNA (PDB ID: 1BNA) dodecamer duplex of sequence d(CGCGAATTCGCG)$_2$.

Cite this: DOI: 10.1039/c0xx00000x

www.rsc.org/xxxxxx

ARTICLE TYPE

Table 4 Molecular docking parameters of the complexes.

Complexes	Final Intermolecular energy (Kcal/mol)			Final Total Internal Energy (Kcal/mol) (2)	Torsional Free Energy (Kcal/mol) (3)	Unbound System's Energy [=(2)] (Kcal/mol) (4)	Estimated Free Energy of Binding [(1)+(2)+(3)-(4)] (Kcal/mol)
	vdW + Hbond + dissolving Energy	Electrostatic Energy	Total (1)				
2	–8.19	–1.11	–9.30	–0.66	+0.82	–0.66	–8.48
5	–10.90	–1.62	–12.51	–3.03	+2.74	–3.03	–9.77

Cytotoxicity evaluation

In vitro cytotoxic activity of all the ligands ($L^{1\&2}$) and complexes (**1**–**6**) was done by MTT [3-(4,5-dimethylthiazol-2-yl)-2,5-diphenyltetrazolium bromide] reduction assay on three different cancer cell lines namely lung (A549), cervical (HeLa) and colon (HCT-15) along with a normal human embryonic kidney (HEK-293) cell line. For cytotoxic activity, four different concentration of compounds (100, 250, 500 and 1000 nM) and cisplatin (positive control) were tested in triplicate for 48 h in two independent experiments. The results are expressed as the average ± standard deviation of two independent experiments. The IC_{50} concentrations of the complexes exhibited differential and dose-dependent inhibitory activity on lung (A549), cervical (HeLa), and colon (HCT-15) cancer cells (**Table 5**).

All the complexes are active against the tested cell lines but the ligand showed no activity. The complexes **1, 2, 3** & **5** exhibited excellent activity against the colon cancer cell line (HCT-15) when compared with the lung (A549) and cervical (HeLa) cancer cells with respect to the standard drug cisplatin. When comparing the inhibitory effect with respect to IC_{50} values, the complexes **2** & **5** show very high activity than the other complexes (**Fig. 12** & **13**). However, complexes exhibited minimum (less than 20%) cytotoxic effect on normal human embryonic kidney cells (HEK-293).

Apoptosis activity of complexes 2 and 5 by live cell and fluorescent imaging

To further address the anticancer activity pattern, the cancer cell lines namely lung (A549), cervical (HeLa) and colon (HCT-15) were treated with respective IC_{50} concentrations of complexes **2** & **5**, the cells were observed in phase contrast microscope and stained with acridine orange-ethidium bromide, which shows dead and floating cells. The acridine orange-ethidium bromide staining shows the morphologic aspect of chromatin condensation in the stained nucleus, allowing one to distinguish viable, apoptotic and necrotic cells. Viable cells possess uniform green nucleus, early apoptotic cells show bright green areas of condensed or fragmented chromatin in the nucleus, and necrotic cells show uniform bright orange nucleus. After staining with acridine orange-ethidium bromide, the cancer cells treated with copper(II) complexes showed apoptotic characteristics such as change in cell morphology, cell shrinkage and nuclear fragmentation, increase in permeability of cell membrane (**Fig. 14**). The results of staining assay demonstrated by the apoptotic features such as nuclear shrinkage, chromatin condensation and nuclear fragmentation after 48 h (**Fig. 15**) showed that complexes **2** & **5** exhibited higher activity against colon (HCT-15) than in lung (A549) and cervical (HeLa) cancer cell lines.

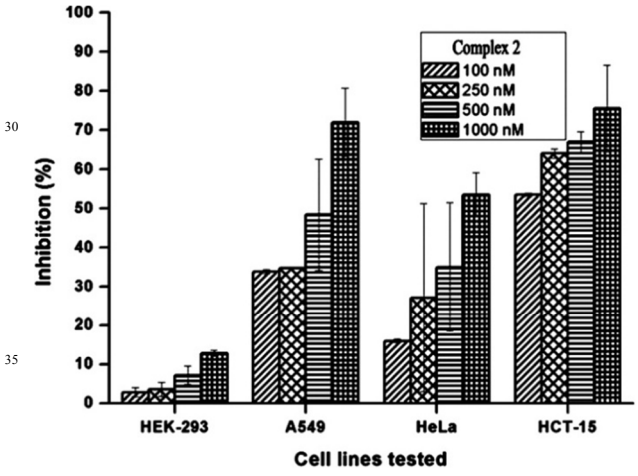

Fig. 12 Cytotoxic activity of complex **2** against non-cancer and cancer cell lines with different concentrations of complex at 48 h.

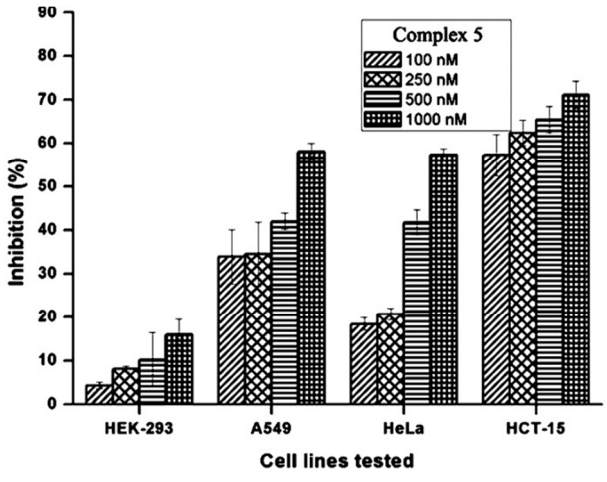

Fig. 13 Cytotoxic activity of complex **5** against non-cancer and cancer cell lines with different concentrations of complex at 48 h

Table 5 [a]IC_{50} values of ligands, complexes and cisplatin against Lung (A549), Cervical (HeLa) and Colon (HCT-15) cancer cells.

Compounds	Lung (A549)	Cervical (HeLa)	Colon (HCT-15)
DMSO	Na*	Na*	Na*
L^1	Na*	Na*	Na*
L^2	Na*	Na*	Na*
1	988±0.14	>1000	120.5±0.22
2	409.4±0.12	521.5±0.1	69.13±0.13
3	438.4±0.4	>1000	166.4±0.26
4	>1000	318.4±0.4	416.3±0.17
5	715.3±0.12	508.9±0.3	33.51±0.16
6	531.7±0.6	978.4±1.2	569.3±0.76
Cisplatin	169±0.8	160.8±1.3	189.3±0.9

[Na*] not active; [a] Inhibitory concentration (IC_{50}) values are derived from dose-response curves obtained by measuring the percentage of viable cells relative to untreated and control after 48 h exposure to test compounds using MTT assay. Values represent means of two independent experiments.

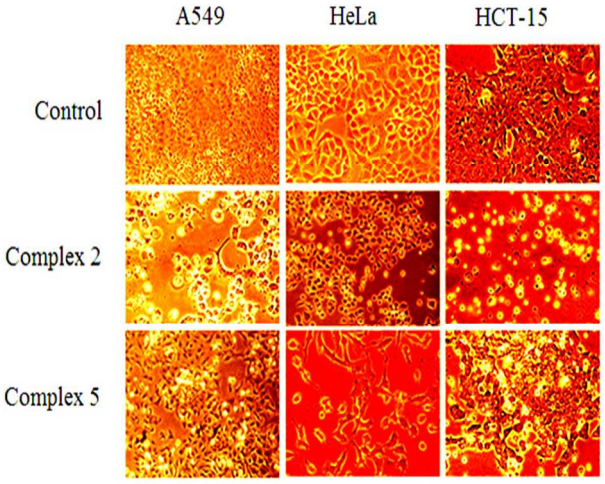

Fig. 14 Live cell imaging of lung (A549), cervical (HeLa) and colon (HCT-15) cancer cells treated with respective IC_{50} concentrations of complexes **2** and **5**.

The mechanism of action is still not completely elucidated. Efforts are continuing to establish the mechanism of action. However, there is evidence that supports the idea that these compounds are able to inhibit cell proliferation and produce dose-dependent cell death by apoptosis. Inhibition of cancer cells and induction of apoptosis might be efficient ways of treating cancer. Apoptosis or programmed cell death involves the activation of energy-requiring intracellular machinery, which is tightly regulated and conserved throughout evolution.[52] Apoptosis eliminates cells exposing the organism to danger. For example, virally infected cells or cells with damaged DNA will be removed by apoptosis.[53] Cancer cells evade apoptosis by several mechanisms. There are two types of apoptosis, death receptor–dependent pathway also called extrinsic pathway and mitochondrial–dependent or intrinsic pathway. Therefore, these complexes have the potential to act as effective metal-based anticancer drugs.

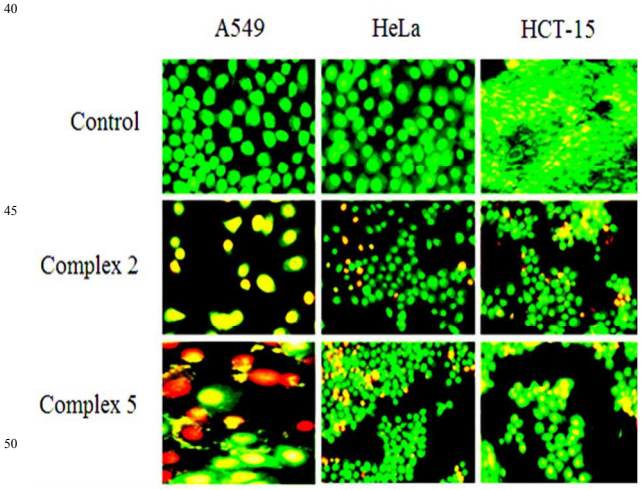

Fig. 15 The morphological changes of lung (A549), cervical (HeLa) and colon (HCT-15) cancer cells treated with respective IC_{50} concentrations of complexes **2** and **5** after stained with acridine orange-ethidium bromide.

Conclusions

Six new complexes of tetrazolo[1,5-*a*]pyrimidine core ligands of type $[ML^1Cl_2]$ (**1**–**3**) and $[M(L^2)_2Cl_2]$ (**4**–**6**) have been synthesized and characterized by spectral methods. The complexes **1**–**3** and **4**–**6** were formed in 1:1 and 1:2 metal-to-ligand mole ratios, respectively. Based on the spectral data square planar geometry was assigned for copper(II) complexes (**2** & **5**) while tetrahedral geometry was assigned for nickel(II) (**1** & **4**) and zinc(II) complexes (**3** & **6**). Single crystal XRD results of complex **6** revealed distorted tetrahedral geometry around the metal ion with two Cl atoms and N atom of two pyridine rings. DNA binding studies revealed that the complexes prefers groove mode of binding; complex **2** binds to CT–DNA through minor groove and complex **5** binds to the major grooves of DNA, which was also supported by molecular docking experiments. The cytotoxicity results showed that complexes selectively inhibited the cancer cells whereas the ligands were found to be inactive against both cancer and non-cancer cell lines. The cytotoxicity of complexes were arranged in the order of **5>2>1** based on the inhibitory effect against colon cells. Furthermore, the apoptotic results of complexes **2** & **5** suggest that these complexes can act as promising anticancer agents for cancer therapy.

Experimental

Materials and methods

Metal(II) chlorides and other commercially available reagents (5-aminotetrazole, sodium thiosulphate, iodine and ethylacetoacetate) were purchased from Aldrich and used without further purification. Solvent for synthesis were reagent grade or better and purified according to standard methods.[54] Calf thymus DNA (CT–DNA) was purchased from Bangalore Genei (India). The melting points were determined using Electro thermal capillary apparatus and they are reported as uncorrected values. Elemental analyses were performed using Carlo Erba model 1106 Elemental analyzer. The FT IR spectra were recorded on a Thermo Nicolet 6700 FT IR spectrometer using KBr pellet in the

range of 400-4000 cm^{-1}. The ^{1}H and ^{13}C NMR spectra were recorded on an a Avans Bruker 400 MHz spectrometer using DMSO-d_6 & $CDCl_3$ as solvent. The mass data of ligands and complexes were obtained on JEOL DX-303 Mass spectrometer and Thermo Finnigan LCQ Advantage MAX 6000 ESI spectrometer, respectively. UV-Vis spectra was recorded on Shimadzu UV-2450 spectrophotometer using acetonitrile as solvent. Fluorescence spectra were recorded on Fluorolog Horiba Jobin Yuvon SPEX-F311 spectrofluorometer. X-band EPR spectra were recorded at 25 ºC on a Varian EPR-E 112 spectrometer using 2,2'-diphenyl-1-picrylhydrazyl (DPPH) as the reference. Room-temperature magnetic studies were performed on a PAR model 155 vibrating-sample magnetometer.

Caution! Metal tetrazolate complexes are potentially explosive. Only a small amount of material should be prepared and handled with caution.

DNA binding experiments

Absorption titrations

All the experiments involving the interaction of complexes with DNA were carried out in Tris-HCl/NaCl buffer (Tris-HCl 5 mM/50 mM NaCl, pH 7.2.). A solution of CT–DNA in the buffer gave a ratio of UV absorbance at 260 and 280 nm, indicating that the DNA was sufficiently free from proteins.[55] The DNA concentration was determined by absorption spectroscopy using the molar absorption coefficient 6600 M^{-1} cm^{-1} at 260 nm.[56] Absorption titration experiment was performed by maintaining the complex concentration constant (10 μM) and varying the concentration of DNA (0-100 μM). While measuring the absorption spectra, equal amounts of DNA was added to both complex solution and the reference solution to eliminate the absorbance of DNA itself. After the addition of DNA to the metal complexes, the resulting solution was allowed to equilibrate at room temperature for 5 min. Then, the sample solution was scanned in the range 200-350 nm. The binding constant (K_b) was determined from the spectroscopic titration data using the following equation.[57]

$$[DNA]/(\varepsilon_a-\varepsilon_f) = [DNA]/(\varepsilon_b-\varepsilon_f) + 1/K_b(\varepsilon_b-\varepsilon_f)$$

Where [DNA] is the concentration of CT–DNA in the base pairs, the apparent absorption coefficient (ε_a) was obtained by calculating A_{obs}/[complex]. The term ε_f, and ε_b correspond to the extinction coefficient of free (unbound) and fully bound compound, respectively. A plot of $[DNA]/(\varepsilon_a - \varepsilon_f)$ *versus* [DNA] will give a slope $1/(\varepsilon_b - \varepsilon_f)$ and an intercept $1/K_b(\varepsilon_b - \varepsilon_f)$. K_b is given by ratio of the slope to the intercept.

Fluorescence spectral studies

For fluorescence quenching experiments, DNA was pretreated with 1% DMF in Tris-HCl/NaCl (pH 7.2) buffer solution as a blank to make preliminary adjustments. The competitive binding experiments were carried out in the buffer by keeping concentration of [DNA]/[EB] = 10 μM constant and varying the concentration of complexes (0–20 μM) at 37 ºC. Before measurements, the mixture was shaken up and incubated at room temperature for 30 min. The fluorescence spectra of EB were measured using an excitation wavelength of 380-460 nm and the emission range was set between 300 and 650 nm. Relative binding of these complexes to CT–DNA is measured from the extent of reduction in emission intensity. The Stern–Volmer quenching constant value was calculated using the equation.[58]

$$I_o/I = 1 + K_{sv}[Q]$$

where I_o is the emission intensity of EB–DNA in the absence of complex, I is the the emission intensity of EB–DNA in the presence of complex, [Q] is the concentration of quencher. K_{sv} is the linear Stern–Volmer constant, obtained as a slope of intercept I_0/I *vs* [Q].

Viscosity experiments

Viscosity experiments were carried out on an Ostwald's viscometer at a constant temperature of 28.0 ± 0.5 ºC in a thermostated bath. Flow time was measured with digital stopwatch for different concentration of complexes (10–50 μM), maintaining the initial DNA concentration (100 μM). Each sample was measured three times and an average flow time was calculated. The DNA viscosity was calculated according to $\eta_i = (t_i - t_o)/t_o$, where η_i is the corresponding values of DNA viscosity; t_i is the flow time of the solution in the presence or absence of the complexes; and t_o is the flow of time buffer alone. Data were presented as $(\eta/\eta_o)^{1/3}$ *versus* binding ratio, where η is the viscosity of DNA in the presence of complex and η_o is the viscosity of DNA alone.[59]

Molecular docking studies

Molecular docking studies have been done using the AutoDock Tools (ADT) version 1.5.6 and AutoDock version 4.2.5.1 docking program. This is an interactive molecular graphics program to understand the drug–DNA interactions to investigate the potential binding mode of complexes. Docking studies were performed by Intel® core i5 CPU (2.53 GHz) with Windows 7 operating system.

DNA Preparation

The X-ray crystal structure of B-DNA (PDB ID: 1BNA) dodecamer $d(CGCGAATTCGCG)_2$ was obtained from the Protein Data Bank (http://www.rcsb.org/pdb). Then the polar hydrogen atoms were added, and ADT was used to remove crystal water, Gasteiger charges were added to each atom, and merged the non-polar hydrogen atoms to the DNA structure. The distance between donor and acceptor atoms that form a hydrogen bond was defined as 1.9 Å with a tolerance of 0.5 Å, and the acceptor–hydrogen–donor angle was not less than 120º. The structures were then saved in PDBQT file format, for further studies in ADT.

Complex preparation

The 2D structures of complexes **2** and **5** were drawn using ChemDraw Ultra 12.0 (ChemOffice 2010) software. Chem3D Ultra 12.0 was used to convert 2D structure into 3D and the energy minimized using semi-empirical AM1 method. Minimize energy to minimum RMS gradient of 0.100 was set in each iteration. All structures were saved as .pdb file format for input to ADT. The structures of complexes were then saved in PDBQT file format to carry out docking in ADT.

Grid formation

Preparation of parameter files for grid and docking was done using ADT. The copper parameters, vdW radii of 0.96 Å and vdW well depth of 0.01 Kcal/mol was used in the docking calculation.[60] A grid box with dimension of 60 × 60 × 110 Å^3 with 0.375 Å spacing and centered on (x,y,z) 14.779, 20.976, 8.804 was created that included the whole DNA using ADT. The center of the box was set at DNA center and grid energy calculations were carried out.

Synthesis of Tetrazolo[1,5-*a*]pyrimidine core ligands

Ethyl 5-methyl-7-pyridine-2-yl-4,7-dihydrotetrazolo[1,5-*a*] pyrimidine-6-carboxylate (L^1)

A mixture of 5-aminotetrazole (0.52 g, 5 mmol), 2-pyridinecarboxaldehyde (0.54 g, 5 mmol) and ethylacetoacetate (0.65 g, 5 mmol) in *iso*-prophyl alcohol (5 mL) was taken in a round bottom flask and iodine (0.13 g, 0.5 mmol) was added to stirred mixture at refluxing temperature (82–85 ºC). After refluxing for 4 h, the whole mixture was cooled to room temperature and added with a solution of sodium thiosulphate (10 M, 2 mL), the solid precipitated was filtered and washed with cold methanol (2 mL) followed by water. The crude product was dried and recrystallized from hot ethanol to afford L^1 as white crystals.

Yield: (1 g, 69.9%). M.p. 260 ºC; Anal. Calc. for $C_{13}H_{14}N_6O_2$ (%): C, 54.57; H, 4.93; N, 29.37; Found: C, 54.52; H, 4.89; N, 29.35. Selected IR data (KBr, υ, cm^{-1}): υ 3246-2937 (br, N-H), 1580 (s, C=N, pyridine ring), 1447 (s, N=N, tetrazole ring), 1701 (s, C=O). ^{1}H NMR (400 MHz: DMSO–d_6 & $CDCl_3$: Me_4Si) δ (ppm): 1.03-1.07 (t, 3H, CH_3 (Et)), 2.42 (s, 3H, -CH_3), 3.93-4.01 (m, 2H, -CH_2Me), 6.63 (s, 1H, -CH-), 7.12-7.15 (t, J = 0.8 Hz, 1H, -C_5H_4N), 7.40-7.42 (d, J = 0.8 Hz, 1H, -C_5H_4N), 7.59-7.65 (m, 1H, -C_5H_4N), 8.35-8.37 (dd, J = 4.0, 0.8 Hz, 1H, -C_5H_4N), 10.91 (s, 1H, -NH). ^{13}C NMR (100 MHz : DMSO–d_6 & $CDCl_3$: Me_4Si) δ (ppm): 164.2, 157.4, 148.8, 148.6, 146.9, 135.8, 122.6, 121.5, 96.3, 59.3, 59.1, 18.2, 13.2. ESI-Mass (*m/z*): 286 ($M^{\cdot+}$, 100.0%), 259 (20), 214 (15).

Ethyl 5-methyl-7-pyridine-4-yl-4,7-dihydrotetrazolo[1,5-*a*] pyrimidine-6-carboxylate (L^2)

The procedure is similar to that of L^1 except that 4-pyridinecarboxaldehyde was used in place of 2-pyridinecarboxaldehyde to afford L^2 as white crystals.
Yield: (1.35 g, 94.0%). M.p. 195 °C; Anal. Calc. for $C_{13}H_{16}N_6O_3$ (%): C, 51.30; H, 5.29; N, 27.61; Found: C, 51.26; H, 5.25; N, 27.60. Selected IR data (KBr, υ, cm^{-1}): υ 3217-2981 (br, N-H), 1553 (s, C=N, pyridine ring), 1433 (s, N=N, tetrazole ring), 1721 (s, C=O). ^{1}H NMR (400 MHz): DMSO–d_6 & $CDCl_3$: Me_4Si) δ (ppm): 1.10-1.14 (t, 3H, CH_3(Et)), 2.65(s, 3H, -CH_3), 4.04-4.12 (m, 2H, -CH_2Me), 6.69 (s, 1H, -CH-), 7.27-7.29 (dd, J = 4.8, 1.6 Hz, 2H, -C_5H_4N), 8.59-8.61 (d-d, J = 4.4, 1.6 Hz, 2H, -C_5H_4N), 11.47 (s, 1H, -NH). ^{13}C NMR (100 MHz : DMSO–d_6 & $CDCl_3$: Me_4Si) δ (ppm): 164.5, 150.1, 148.7, 148.3, 147.4, 122.2, 97.5, 60.8, 58.3, 19.4, 14.0. ESI-Mass (*m/z*): 305.3 ($M^{\cdot+}$+H, 100.0%), 259 (25), 214 (15).

General procedure for synthesis of mononuclear nickel(II), copper(II) and zinc(II) complexes

To a methanolic solution (25 mL) of ligands L^1 (1.36 mmol)/ L^2 (2.72 mmol) was added a methanolic solution (25 mL) of metal(II) chloride (1.36 mmol) under constant stirring. Then, the reaction mixture was refluxed for 2 h, filtered hot and allowed to stand at room temperature for 7 days. The crystalline product obtained was washed with cold methanol and dried in *vacuuo*.

(Ethyl 5-methyl-7-pyridine-2-yl-4,7-dihydrotetrazolo[1,5-*a*] pyrimidine-6-carboxylato)dichloronickel(II) complex [NiL^1Cl_2], (1)

Yield: (0.36 g, 64.10%). Green solid. Anal. Calc. for $C_{13}H_{14}N_6O_2Cl_2Ni$ (%): C, 37.72; H, 3.40; N, 20.30; Found: C, 37.69; H, 3.38; N, 20.29. Selected IR data (KBr, υ, cm^{-1}): υ 3249-2978 (br, N-H), 1560 (s, C=N, pyridine ring), 1429 (s, N=N, tetrazole ring), 1706 (s, C=O). UV-Vis [(λ_{max} (nm) (ε, dm^{3}mol^{-1}cm^{-1})] in CH_3CN: 249 (11, 400), 462 (590). ESI-Mass (*m/z):* 415 ([NiL^1Cl_2]$^+$; 40%), 380 ([NiL^1Cl]$^+$; 60%), 344 ([NiL^1]$^+$; 50%), 287 ([L^1]$^+$+H ; 90%). μ_{eff}: 3.33 BM.

(Ethyl 5-methyl-7-pyridine-2-yl-4,7-dihydrotetrazolo[1,5-*a*] pyrimidine-6-carboxylato)dichlorocopper(II) complex [CuL^1Cl_2], (2)

Yield: (0.40 g, 70.37%). Green solid. Anal. Calc. for $C_{13}H_{14}N_6O_2Cl_2Cu$ (%): C, 37.27; H, 3.36; N, 20.06; Found: C, 37.24; H, 3.34; N, 20.05. Selected IR data (KBr, υ, cm^{-1}): υ 3096-2978 (br, N-H), 1559 (s, C=N, pyridine ring), 1420 (s, N=N, tetrazole ring), 1705 (s, C=O). UV-Vis [(λ_{max} (nm) (ε, dm^{3}mol^{-1}cm^{-1})] in CH_3CN: 259 (7,816), 307 (7,400), 464 (1580). $g_{\|}$: 2.20, g⊥: 2.09 and $A_{\|}$: 184.33. ESI-Mass (*m/z):* 420.55 ([CuL^1Cl_2]$^+$; 40%), 385 ([CuL^1Cl]$^+$; 70%), 349 ([CuL^2]$^+$; 40%), 286 ([L^1]$^+$; 75%). μ_{eff}: 1.88 BM.

(Ethyl 5-methyl-7-pyridine-2-yl-4,7-dihydrotetrazolo[1,5-*a*] pyrimidine-6-carboxylato)dichlorozinc(II)complex [ZnL^1Cl_2], (3)

Yield: (0.30 g, 52.65%). Colourless solid. Anal. Calc. for $C_{13}H_{14}N_6O_2Cl_2Zn$ (%): C, 37.18; H, 3.36; N, 20.01; Found: C, 37.15; H, 3.33; N, 20.00. Selected IR data (KBr, υ, cm^{-1}): υ 3246-2963 (br, N-H), 1560 (s, C=N, pyridine ring), 1429 (s, N=N, tetrazole ring), 1706 (s, C=O). ^{1}H NMR (400 MHz: DMSO–d_6& $CDCl_3$: Me_4Si) δ (ppm): 1.03-1.07 (t, 3H, CH_3(Et)), 2.41 (s, 3H, -CH_3), 3.93-4.03 (m, 2H, -CH_2Me), 6.69 (s, 1H, -CH-), 7.23-7.26 (t, J = 0.8 Hz, 1H, -C_5H_4N), 7.51-7.53 (d, J = 8.0 Hz, 1H, -C_5H_4N), 7.73-8.16 (m, 1H, -C_5H_4N), 8.40 (dd, J = 4.8, 0.8 Hz, 1H, -C_5H_4N), 11.16 (s, 1H, -NH). ^{13}C NMR (100 MHz): DMSO–d_6 & $CDCl_3$: Me_4Si) δ (ppm): δ 164.4, 158.2, 149.5, 149.2, 147.1, 136.6, 123.4, 122.3, 96.9, 59.5, 18.5, 13.8. UV-Vis [(λ_{max} (nm) (ε, dm^{3}mol^{-1}cm^{-1})] in CH_3CN: 275 (15,000). ESI-Mass (*m/z):* 422.70 ([ZnL^1Cl_2]$^+$; 40%), 387 ([ZnL^1Cl]$^+$; 60%), 351 ([ZnL^1]$^+$; 70%), 286 ([L^1]$^+$; 65%).

Bis(Ethyl 5-methyl-7-pyridine-4-yl-4,7-dihydrotetrazolo[1,5-*a*] pyrimidine-6-carboxylato)dichloronickel(II)complex $[Ni(L^2)_2Cl_2]$, (4)

Yield: (0.75 g, 77.31%). Yellowish green solid. Anal. Calc. for $C_{26}H_{28}N_{12}O_4Cl_2Ni$ (%): C, 44.60; H, 4.03; N, 24.00; Found: C, 44.56; H, 3.99; N, 23.99. Selected IR data (KBr, υ, cm^{-1}): υ 3010-2966 (br, N-H), 1520 (s, C=N, pyridine ring), 1430 (s, N=N, tetrazole ring), 1720 (s, C=O). UV-Vis [(λ_{max} (nm) (ε, $dm^3mol^{-1}cm^{-1}$)] in CH_3CN: 274 (13,600), 470 (490). ESI-MS (*m/z):* 703 ($[Ni(L^3)_2Cl_2^+$ +1H; 50%), 665 ($[Ni(L^3)_2Cl^+$; 95%), 629 ($[Ni(L^3)_2^+$; 15%). μ_{eff}: 3.35 BM.

Bis(Ethyl 5-methyl-7-pyridine-4-yl-4,7-dihydrotetrazolo[1,5-*a*]pyrimidine-6-carboxylato)dichlorocopper(II) complex $[Cu(L^2)_2Cl_2]$, (5)

Yield: (0.84 g, 86.59%). Green solid. Anal. Calc. for $C_{26}H_{28}N_{12}O_4Cl_2Cu$ (%): C, 44.28; H, 4.00; N, 23.83; Found: C, 44.24; H, 3.97; N, 23.82. Selected IR data (KBr, υ, cm^{-1}): υ 3190-2928 (br, N-H), 1502 (s, C=N, pyridine ring), 1430 (s, N=N, tetrazole ring), 1719 (s, C=O). UV-Vis [(λ_{max} (nm) (ε, $dm^3mol^{-1}cm^{-1}$)] in CH_3CN: 260 (7,600), 310 (7,500), 472 (1,430). $g_{\|}$: 2.16, $g_{\perp}$: 2.05 and $A_{\|}$: 183.02. ESI-MS (*m/z):* 717 ($[Cu(L^3)_2Cl_2]^+$; 25%), 25%), 671 ($[Cu(L^3)_2Cl^+$; 636 ($[Cu(L^3)_2^+$; 25%). μ_{eff}: 1.93 BM.

Bis(Ethyl 5-methyl-7-pyridine-4-yl-4,7-dihydrotetrazolo[1,5-*a*]pyrimidine-6-carboxylato)dichlorozinc(II) complex $[Zn(L^2)_2Cl_2]$, 6

Yield: (0.75 g, 76.49%). Colourless solid. Anal. Calc. for $C_{28}H_{37}N_{12}O_{6.5}Cl_2Zn$ (%): C, 43.00; H, 4.76; N, 21.49; Found: C, 42.96; H, 4.73; N, 21.48. Selected IR data (KBr, υ, cm^{-1}): υ 3243-2934 (br, N-H), 1530 (s, C=N, pyridine ring), 1431 (s, N=N, tetrazole ring), 1720 (s, C=O). ^1H NMR (400 MHz: DMSO–d_6 & $CDCl_3$: Me_4Si) δ (ppm): 1.07 (t, 3H, CH_3(Et)), 2.52-2.54 (s, 6H, -$(CH_3)_2$), 3.21 (s, 3H, Solvent CH_3OH), 4.02-4.13 (m, 4H, -$(CH_2Me)_2$), 6.75 (s, 1H, -CH-), 7.41 (s, 2H, -C_5H_4N), 8.61 (s, 2H, -C_5H_4N), 11.45 (s, 1H, -NH). ^{13}C NMR (100 MHz: DMSO–d_6 & $CDCl_3$: Me_4Si) δ (ppm): 164.3, 150.1, 149.0, 148.4, 147.7, 122.3, 96.3, 59.8, 57.7, 48.6 (solvent CH_3OH), 18.5, 13.7. UV-Vis [(λ_{max} (nm) (ε, $dm^3mol^{-1}cm^{-1}$)] in CH_3CN: 290 (11,900). ESI-MS (*m/z):* 782.1 ($[Zn(L^3)_2Cl_2{:}2CH_3OH{:}1/2H_2O]^+$; 60%), 673 ($[Zn(L^3)_2Cl]^+$; 40%), 637 ($[Zn(L^3)_2]^+$; 70%).

Cell culture

Human lung (A549), cervical (HeLa), colon (HCT-15) cancer cell lines and human embryonic kidney (HEK) non-cancer cell lines were obtained from National Centre for Cell Science (NCCS), Pune, India. The lung (A549), cervical (HeLa), colon (HCT-15) and human embryonic kidney (HEK) cells were maintained in Dulbecco's Modified Eagle's Medium (DMEM) while the colon (HCT-15) was maintained in Roswell Park Memorial Institute Medium (RPMI) supplemented with 10% fetal bovine serum (FBS), 10 mg/mL of penicillin, 10 mg/mL of streptomycin, and 0.25 mg/mL of amphotericin B at 37 ºC at 5% CO_2 incubator.

MTT Assay

The cytotoxicity or survival of cells in the presence or absence of the experimental agents was determined using MTT assay as described previously by Mosmann.[61] Briefly, human lung (A549), cervical (HeLa) and colon (HCT-15) cancer and human embryonic kidney (HEK) non-cancer cells were seeded at the density of 6000 cells per well in 96 well plates for 24 h, in 200 µL of DMEM supplemented with 10% FBS. Different concentration of complexes (100-1000 nM) were treated in triplicates and incubated for 48 h at 37 °C in 5% CO_2 incubator. After treatment, cells were incubated with MTT (10 µL; 5 mg/mL) at 37 °C for 3 h and formazan crystals formed was dissolved in 80 µL of DMSO. The plates were read at 590 nm on a scanning multiwell spectrophotometer and the IC_{50} (concentration of compounds to kill 50% of the cells) values was obtained by dose-response curve using Graph pad prism software and the graph was plotted against percentage of cell inhibition *versus* concentration using origin 6.0 software. The statistical significance of the data was analysed by ANNOVA with the level of significance, $p<0.05$. To clarify any participating role of DMSO in the cancer and non-cancer cell lines, separate studies were carried out with the solution of DMSO and they showed no activity against all cancer and non-cancer cell lines.

Apoptosis assessment by live cell imaging and acridine orange-ethidium bromide staining.

For live cell imaging, the cancer cell lines were treated with respective IC_{50} concentrations of copper(II) complexes (**2** & **5**) for 48 h and morphology of cells was observed under invert phase contrast microscope. For fluorescent imaging, after treatment, the cancer cells were stained with freshly prepared Acridine orange/Ethidium bromide staining solution (100 µg/mL) and observed under fluorescent microscope (Olympus BX-51) within less than 20 min.

X-Ray crystallography

X-ray diffraction studies for ligands ($L^{1\&2}$) and complex **6** were carried out using a Bruker AXS Kappa APEX II single crystal CCD diffractometer equipped with graphite-monochromated Mo (Kα) (λ = 0.71073 Å) radiation. The goniometer equipped with the diffractometer is four circle goniometer with φ, χ, ω and 2θ axes by which the crystal is rotated. The intensity data were collected using ω and φ scans with frame width 1°. For all compounds, data collection and data reduction was done using APEX2, SAINT/XPREP software (version 7.06a). The multi-scan absorption correction was done using SADABS program.[62] The structures was solved by direct methods using SHELXS97 and refined using SHELXL97 by the methods of full-matrix least squares refinement.[63] The molecular graphics were done using ORTEP-3.[64]

Supporting Information

Crystallographic data for ligands ($L^{1\&2}$) and complex **6** have been deposited with the Cambridge Crystallograpic Data Centre (CCDC) as supplementary publication numbers CCDC-881456, CCDC-881461 and CCDC-873831. The data can be obtained free of charge from http://www.ccdc.cam.ac.uk/conts/retrieving.html or from the CCDC (12 Union Road, Cambbridge CB2 1EZ, UK; Fax: +44-1223-336033; e-mail: deposit@ccdc.cam.ac.uk). Table S1 show crystal data and structure refinement for ligands $L^{1\&2}$

and complex **6**, Table S2-S5 show the data of bond length, bond angle and hydrogen bond parameters for ligands $L^{1\&2}$, Figures S1-S4 show crystal packing and hydrogen bonding parameter of ligands $L^{1\&2}$, Figures S5-S8 show FT IR spectra of ligands $L^{1\&2}$ and complexes **1** and **4**. Figures S9-S16 show ^{1}H and ^{13}C NMR spectra of ligands $L^{1\&2}$ and complexes **3** and **6**. Figure S17 shows UV-Vis spectra of complexes **1** and **2** and Figure S18 shows X-band EPR spectrum of complex **2.**

Notes and references

[a] *Post-Graduate and Research Department of Chemistry, The New College (Autonomous), Chennai-600 014, India. Fax: +91 44 2835 2883; Tel.: +91 44 2835 029; E-mail: akrahmanjkr@gmail.com.*
[b] *Department of Chemistry, Pondicherry University, Pondicherry-605 014, India.*
[c] *Department of Biotechnology, Pondicherry University, Pondicherry-605 014, India.*
[d] *Organic Chemistry Division, CSIR-Central Leather Research Institute, Chennai-600020, India.*

† Electronic Supplementary Information (ESI) available: [details of any supplementary information available should be included here]. See DOI: 10.1039/b000000x/

References

1 W. G. Finnegan, R. A. Henry and R. Lofquist, *J. Am. Chem. Soc*., 1958, **80**, 3908–3911.
2 B. E. Huff and M. A. Staszak, *Tetrahedron Lett.,* 1993, **34**, 8011–8014.
3 A. Kumar, R. Narayanan and H. Shechter, *J. Org. Chem*., 1996, **61**, 4462–4465.
4 Z. P. Demko and K. B. Sharpless, *J. Org. Chem*., 2001, **66**, 7945–7950.
5 H. Zhao, Z. R. Qu, H. Y. Ye and R. G. Xiong, *Chem. Soc. Rev*., 2008, **37**, 84–100.
6 L. Z. Wang, Z. R. Qu, H. Zhao, X. S. Wang, R. G. Xiong and Z. L. Xue, *Inorg. Chem*., 2003, **42**, 3969–3971.
7 X. H. Mo, E. Q. Gao, Z. He, W. J. Li and C. H. Yan, *Inorg. Chem. Commun*., 2004, **7**, 353–355.
8 J. Clark, M. S. Shahhet, D. Korakas and G. Varvounis, *J. Heterocycl. Chem*., 1993, **30**, 1065–1072.
9 B. J. A. Hourani, S. K. Sharma, M. Suresh and F. Wuest, *Bioorg. Med. Chem. Lett*., 2012, **22**, 2235–2238.
10 C. Bulow, *Ber*. 1909, **42**, 4429– 4438.
11 A. M. Hussein and O. M. Ahmed, *Bioorg. Med. Chem*., 2010, **18**, 2639–2644.
12 A. Terenzi, G. Barone, A. Palumbo Piccionello, G. Giorgi, A. Guarcello, P. Portanova, G. Calvaruso, S. Buscemi, N. Vivona and A. Pace. *Dalton Trans*., 2010, **39**, 9140–9145.
13 R. G. Xiong, X. Xue, H. Zhao, X. Z. You and Z. Xue, *Angew. Chem. Int. Ed*., 2002, **41**, 3800–3803.
14 M. Cocchi, J. Kalinowski, S. Stagni and S. Muzzioli, *Appl. Phys. Lett*., 2009, **94**, 0833061–0833063.
15 H. Zhao, Z. R. Qu, H. Y. Ye and R. G. Xiong, *Chem. Soc. Rev*., 2008, **37**, 84–100.
16 L.-Z. Wang, Z.-R. Qu, H. Zhao, X.-S. Wang, R.-G. Xiong and Z.-L. Xue*, Inorg. Chem*., 2003, **42**, 3969–3971.
17 L. -Y. Zeng and C. Cai, *J. Comb. Chem*., 2010, **12**, 35–100.
18 C. S. Yao, C. X. Yu, L. Song and S. J. Tu, *Acta. Cryst*., 2007, **E63**, o3808.
19 C. Jiang, Z. Yu, S. Wang, C. Jiao, J. Li, Z. Wang and Y. Cui, *Eur. J. Inorg. Chem*., 2004, **18**, 3662–3667.
20 J. M. Seco, M. D. A. Farias, N. M. Bachs, A. B. Caballero, A. S. Castillo and A. R. Dieguez, *Inorg. Chim. Acta*., 2010, **363**, 3194–3199.
21 A. P. Mosalkova, S. V. Voitekhovich, A. S. Lyakhov, L. S. Ivashkevich, P. N. Gaponik and O. A. Ivashkevich, *Z. Anorg. Allg. Chem*., 2012, **638**, 103–110.
22 M. M. Degtyarik, P. N. Gaponik, V. N. Naumenko, A. I. Lesnikovich and M. V. Nikanovich, *Spectrochim. Acta*., 1987, **43**, 349–353.
23 S. B. Lara, C. G. Ruiz, L. R. B. Sosa, I. G. Mora, M. F. Alamo and N. B. Behrens, *J. Inorg. Biochem*., 2012, **114**, 82–93.
24 E. Budzisz, I. P. Lorenz, P. Mayer, P. Paneth, L. Szatkowshi, U. Krajewska, M. Rozalski and M. Miernicka, *New. J. Chem*., 2008, **32**, 2238–2244.
25 M. Amirnasr, A. H. Mahmoudkhani, A. Gorji, S. Dehghanpour and H. R. Bijanzadeh, *Polyhedron*, 2002, **21**, 2733–2742.
26 A. B. P. Lever, Inorganic Electronic Spectroscopy, Elsevier, Amsterdam, 2nd ed: 1984, pp.496.
27 S. V. Voitekhovich, T. V. Serebryanskaya, A. S. Lyakhov, P. N. Gaponik and O. A. Ivashkevich, *Polyhedron*, 2009, **28**, 3614–3620.
28 R. Pandey, J. Ribas, M. Corbella and D. S. Pandey, *Indian J. Chem*., 2011, **50A**, 1450–1456.
29 T. Hu, L. Liu, X. Lv, X. Chen, H. He, F. Dai, G. Zhang and D. Sun, *Polyhedron*, 2010, **29**, 296–302.
30 Y. Z. Tang, G. X. Wang, Q. Ye, R. G. Xiong and R. X. Yuan, *Cryst. Growth Des*., 2007, **7**, 2382–2386.
31 Z. F. Chen, R. G. Xiong, J. Zhang, X. T. Chen, Z. L. Xue and X. Z. You, *Inorg. Chem*., 2001, **40**, 4075–4077.
32 B. Liu, Y. C. Qiu, G. Peng, L. Ma, L. M. Jin, J. B. Cai and H. Deng, *Inorg. Chem. Commun*., 2009, **12**, 1200–1203.
33 B. J. Hathaway and A. A. G. Tomlinson, *Coord. Chem. Rev*., 1970, **5**, 1–143.
34 A. H. Maki and B. R. McGarvey, *J. Chem. Phys*., 1958*,* **29**, 31–34.
35 D. Kivelson and R. Neiman, *J. Chem. Soc. Dalton Trans*., 1961, **35**, 149–155.
36 R. P. John, A. Sreekanth, V. Rajakannan, T. A. Ajith and M. R. P. Kurup, *Polyhedron,* 2004, **23**, 2549–2559.
37 E. B. Seena, R. Maliyeckal and P. Kurup, *Polyhedron,* 2007, **26**, 829– 836.
38 R. V. Parish, NMR, NQR, EPR and Mössbauer spectroscopy in Inorganic Chemistry; Ellis Horwood Limited: vol. 2, 1990, pp.10–20.
39 A. D. Kulkarni, S. A. Patil, V. H. Naik and P. S. Badami, *Med. Chem. Res*., 2011, **20**, 346–354.
40 A. L. Nivorozhkin, H. Toftlund, L. E. Nivorozhkin, I. A. Kamenetskaya, A. S. Antsishkina and M. A. Porai-Koshits, *Transition Met. Chem*., 1994, **19**, 319–324.
41 P. Kumar, B. Baidya, S. M. Chaturvedi, R. H. Khan, D. Manna and B. Mondal. *Inorg. Chim. Acta,* 2011, **376**, 264–270.
42 H. L. Chan, Q. L. Liu, B. C. Tzeng, Y. S. You, S. M. Peng, M. Yang and C. M. Che, *Inorg. Chem*., 2002, **41**, 3161–3171.
43 S. Neidle, *Nat. Prod. Rep*., 2001, **18**, 291–309.
44 Y. Takeda, D. H. Ohlendorf, W. F. Anderson and B. W. Matthews, *Scinece*, 1983, **221**, 1020–1026.
45 F. Arjmand and S. Parveen. *RSC. Adv*., 2012, **2**, 6354–6362.
46 P. Sathyadevi, P. Krishnamoorthy,N. S. P. Bhuvanesh, P. Kalaiselvi, V. V. Padma and N. Dharmaraj, *Eur. J. Med. Chem*., 2012, **55**, 420–431.
47 J. B. Chaires, *Biopolymer*, (Nucleic Acid Sci.) 1998, **44**, 201–215.
48 M. T. Record, C. F. Anderson, T. M. Lohman and Q. Rev, *Biophys*., 1978, **11**, 103–178.
49 P. U. Maheswari, V. Rajendiran, H. S. Evans and M. Palaniandavar, *Inorg. Chem*., 2006, **45**, 37–50.
50 S. Ramakrishnan, E. Suresh, A. Riyasdeen, M. A. Akbarsha and M. Palaniandavar, *Dalton Trans*., 2011, **40**, 3524–3536.
51 P. Yang and M. Guo, *Met.-Based Drugs*, 1998, **5**, 41–58.
52 J. Y. Yuan, *J. Cell Biochem*., 1996, **60**, 4–11.
53 D. R. Green and S. J. Martin, *Curr. Opin. Immunol*., 1995, **7,** 694–703.
54 W. L. F. Armarego and D. D. Perrin, Purification of Laboratory Chemicals, fourth ed., Pergamon press, 1996. Bruker AXS Inc., Madison, Wisconsin, USA, 2004.
55 J. Marmur, *J. Mol. Bio*., 1961, **3**, 208–218.
56 M. E. Reichmann, S. A. Rice, C. A. Thomas and P. Doty, *J. Am. Chem. Soc*., 1954, **76**, 3047–3053.
57 O. Stern and M. Volmer, *Phys. Z.* 1919, **20**, 183–188.

58 A. Wolfe, G. H. Shimer and T. Meehan, *Biochemistry*, 1987, **26**, 6392–6396.
59 G. Cohen and H. Eisenberg, *Biopolymers*, 1968, **6**, 1077–1100.
60 K. Zheng, M. Jiang, Y.-T. Li, Z.-Y. Wu and C.-W. Yan, *J. Mol. Struct*., 2014, **1058**, 97–105.
61 T. Mosmann, *J. Immunol. Methods*, 1983, **65**, 55–63.
62 Bruker-Nonius, APEX-II and SAINT-Plus (Version 7.06a),
63 G.M. Sheldrick, SHELX-97, Program for x-ray Crystal Structure Solution and Refinement, University of Gottingen, Germany, 1997.
64 L. J. Farrugia, *J. Appl. Crystallogr*., 1997, **30**, 565–566.